J Solid State Electrochem (2016) 20:3071–3081
DOI 10.1007/s10008-016-3298-0

ORIGINAL PAPER

Glassy carbon electrode modified with hemin and new melamine compounds for H_2O_2 amperometric detection

Aglaia Raluca Deac[1] · Cristina Morar[2] · Graziella Liana Turdean[1] · Mircea Darabantu[2] · Emese Gál[3] · Attila Bende[4] · Liana Maria Muresan[1]

Received: 8 March 2016 / Revised: 22 May 2016 / Accepted: 17 June 2016 / Published online: 24 June 2016

Abstract In an attempt to increase the stability and efficiency of hemin-modified electrodes, the present work reports the preparation of a new modified glassy carbon electrode obtained by immobilization of hemin (**Hm**) on the electrode surface together with a new *N*-substituted melamine (2,4,6-triamino-1,3,5-triazine) based G-2 dendrimer comprising *p*-aminophenol as peripheral unit (**Den**) or with one of its analogues, a melamine G-0 dimer (**Dim**). Basic structural features, able to determine intimate relationships between **Hm** and **Dim** (or **Den**) at room temperature in solid state, were evidenced with the use of vibrational analysis carried out by FT-IR. This method revealed contacts between **Hm** and **Dim** or **Den** respectively as H-bond interactions, proton-interchange, and π-π stacking interactions. The new modified electrodes were characterized by cyclic voltammetry and electrochemical impedance spectroscopy and tested for amperometric detection of H_2O_2. In this purpose, **GC/Hm-Dim** electrode exhibited better catalytic properties than **GC/Hm-Den** electrode, but lower stability.

Keywords Hemin-modified electrodes · Dendritic melamines · Cyclic voltammetry · Electrochemical impedance spectroscopy · Amperometric detection of H_2O_2

Introduction

The detection of low levels of hydrogen peroxide (H_2O_2) is of particular interest for modern medicine, environmental control, and various branches of industry. Among the catalysts used for H_2O_2 detection, hemin (**Hm**) is efficient as mediator based on the reversible Fe(III)/Fe(II) redox couple present in its structure.

This functionality makes this minizyme very attractive for bioelectronic and bioelectrochemical sensors applications [1–3].

Hemin is a well-known protoporphyrin IX containing a ferric iron ion (heme B) with a chloride ligand. However, the direct use of hemin as a redox catalyst in aqueous media is still a challenging task because of its aggregation leading to inactive dimers [4]. As a consequence, the electrochemical stability of hemin modified electrodes is, usually, unsatisfactory [1]. Therefore, in order to ensure good sensing performances of the electrodes, a smart immobilization of hemin on substrates is necessary.

Various methods have been used to realize hemin-modified electrodes, such as entrapment in a polymeric matrix [5, 6], adsorption on different carbon nanomaterials [3, 7], drop casting [1], layer-by-layer deposition [8], incorporation in carbon paste [9], etc. Nevertheless, other new alternatives should be investigated in order to increase the performances of the hemin-based electrodes.

Electronic supplementary material The online version of this article (doi:10.1007/s10008-016-3298-0) contains supplementary material, which is available to authorized users.

✉ Liana Maria Muresan
limur@chem.ubbcluj.ro

[1] Department of Chemical Engineering, "Babes-Bolyai" University, Cluj-Napoca, Romania

[2] Department of Chemistry, "Babes-Bolyai" University, Cluj-Napoca, Romania

[3] Department of Chemistry and Chemical Engineering, Hungarian Line of Study, "Babes-Bolyai" University, 11 Arany János St., Cluj-Napoca 400028, Romania

[4] Molecular and Biomolecular Physics Department, National Institute for Research and Development of Isotopic and Molecular Technologies, 65-103, Donath St., PO Box 700, Cluj-Napoca 5 400293, Romania

Dendrimers are attracting increased attention nowadays because of their unique structures and properties [10]. Dendrimers are branched macromolecules with a fractal structure that exhibit a high degree of constitutional order, with the possibility of containing selected chemical units at predetermined sites of their molecules [11]. The dendritic architecture can serve as a versatile platform for *host-guest* interactions, e.g., in the design of novel encapsulation agents [12], and/or surface interactions with oppositely charged molecules [13]. Dendrimer-modified surfaces can potentially be applied as catalysts with multiple redox reaction centers [14], being well suited to modify electrode surfaces and to support charge-transfer mediators [15]. On the other hand, except our previous reports [16, 17], so far almost no attention was paid to dendritic melamines' electrochemical behavior.

In this context, aiming at increasing the stability and efficiency of hemin-modified electrodes, the present work reports the preparation of a new glassy carbon electrode modified by hemin immobilized on the electrode surface together with a new *N*-substituted melamine (2,4,6-triamino-1,3,5-triazine) based G-2 dendrimer comprising *p*-aminophenol as peripheral unit or with one of its analogues, a melamine G-0 dimer.

By enhancing the hydrophobic nature of the electrode-solution interface and by stabilizing and concentrating the mediator (hemin), the use of two new *N*-substituted melamines (a dimeric G-0 dendron and a G-2 dendrimer) comprising *p*-aminophenol as peripheral unit aims at improving the electrochemical and electroanalytical properties of the hemin modified electrodes. The new modified electrodes were characterized with the use of cyclic voltammetry and electrochemical impedance spectroscopy and tested for amperometric detection of H_2O_2. Moreover, a better understanding of the intimate interactions between the different organic molecules present on the electrode surface was also acquired.

Experimental

Reagents

The 98 % purity iron(III) protoporphyrin IX chloride (Hemin, **Hm**), having the formula presented in Scheme 1, was purchased from Fluka, Switzerland.

The compounds used in this study to immobilize **Hem**in (**Hm**) on the surface of the GC electrode were a **Dim**eric melamine G-0 dendron (**Dim**) and a G-2 melamine **Den**drimer (**Den**) (Scheme 2) [17] (for the present work, see Supplementary material their NMR and HRMS characterization).

Hydrogen peroxide, (H_2O_2), $Na_2HPO_4{\cdot}2H_2O$, and $NaH_2PO_4{\cdot}H_2O$ were obtained from Merck (Darmstadt, Germany). All reagents were of analytical grade and used as received. The supporting electrolyte for electrodes testing was

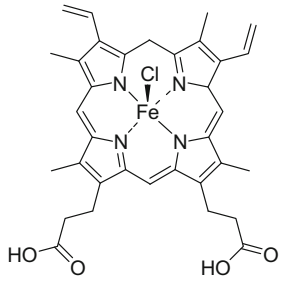

Hemin (**Hm**)
[Chloro(protoporphyrinato)iron
Ferriprotoporphyrin IX chloride
Iron(III) protoporphyrin chloride]

Scheme 1 Structural formula of hemin

0.1 M phosphate buffer solution (pH 7) obtained by mixing appropriate solutions of $Na_2HPO_4{\cdot}2H_2O$ and $NaH_2PO_4{\cdot}H_2O$. A solution of 0.1 M KCl containing 0.05 M $K_3[Fe(CN)_6]$/$K_4[Fe(CN)_6]$ was prepared by dissolving an appropriate weight of salts supplied by Aldrich-Sigma in distilled water and used to investigate the accessibility of the electrode's surface.

DMSO (Merck, Darmstadt, Germany) was used as solvent for the melamine compounds.

Apparatus and methods

Voltammetric measurements were performed using a PGSTAT 12/100, Booster 20A, electrochemical station (AUTOLAB, The Netherlands). A pH-meter (MV 870 PRACITRONIC, Germany) equipped with a combined glass electrode was used to measure the pH of solutions. For shaking the solutions, a vortex mixer (100–3000 rpm from Falc Instruments) was used. A three-electrode electrochemical cell consisting of a working electrode (glassy carbon) with inner diameter of 3 mm, a Pt counter electrode, and an Ag/AgCl/KCl_{sat} reference electrode has been used for all experimental measurements.

Amperometric measurements were performed at applied potential of −0.35 V versus Ag/AgCl, KCl_{sat} under continuous stirring of electrolyte, by repetitive addition of 50 μL from a 10^{-2} M H_2O_2 stock solution in 10 mL buffer solution.

The *ac* impedance analysis was carried out in a frequency range from 10 kHz to 0.01 Hz at room temperature, by immersion of **GC/Hm**, **GC/Dim**, **GC/Dim-Hm**, **GC/Den**, and **GC/Den-Hm** modified electrodes in 0.1 M KCl containing 0.05 M $[Fe(CN)_6]^{3-}/[Fe(CN)_6]^{4-}$. The EIS spectra were recorded at 10 points per hertz decade with an AC voltage amplitude of ±10 mV. The applicability of the models used for the fitting procedure of the spectra was confirmed by the chi-square (χ^2) values that were typically lower than 10^{-3}.

For vibrational analysis, two DMSO solutions, containing mixtures **Hm-Dim** or **Hm-Den** in 5:1 molar ratio, respectively, were lyophilized. The resulted solids were analyzed by FT-

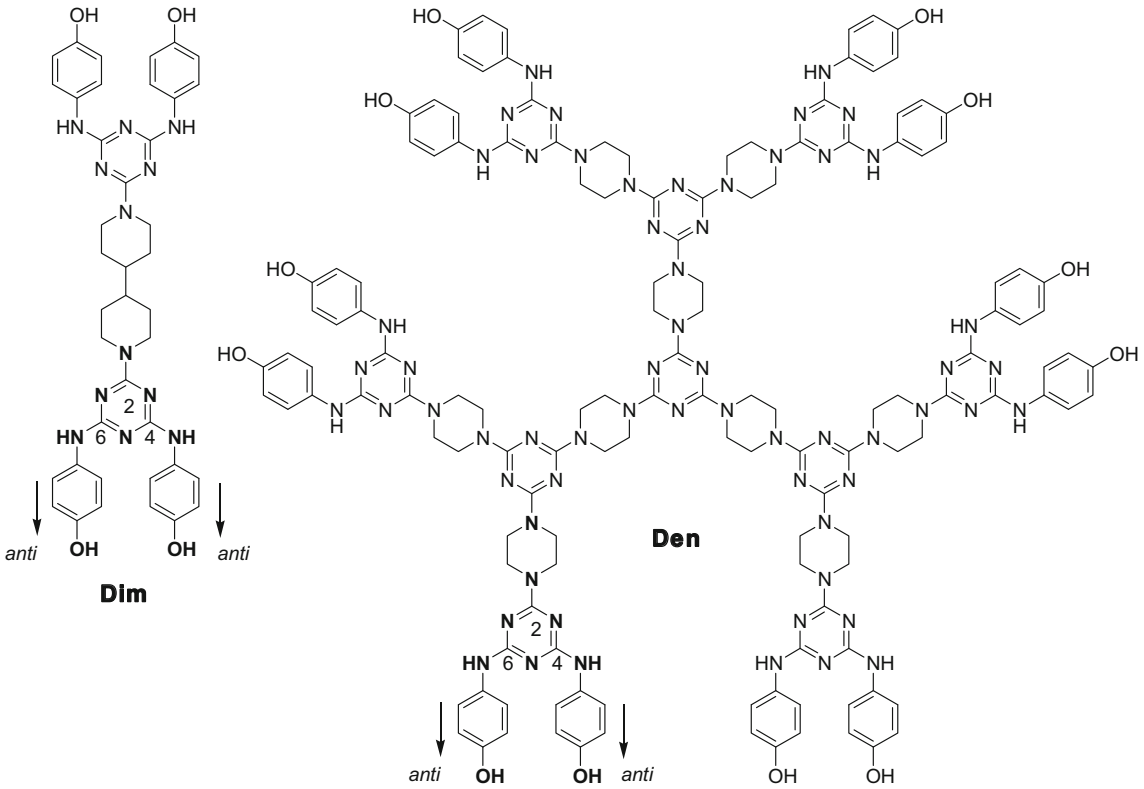

Scheme 2 Structural formula of the melaminic dimer (**a**) and dendrimer (**b**)

IR spectroscopy carried out on a FT-IR Bruker Vektor 22 spectrometer.

Preparation of the modified electrodes

Before modification, the glassy carbon (BAS Inc., USA) working electrode was wet polished to a mirror-like finish on wet fine (grit 1200 and 2000) emery paper and felt with alumina slurry (Buehler, Lake Bluff, IL, USA), and then sonicated for 30 min.

Stock solutions of 10^{-3} M of **Dim**, **Den**, and **Hm** were each prepared by dissolving appropriate amounts into DMSO. Standard solution of 5 mM **Hm-Dim** and **Hm-Den** were prepared by dissolving the appropriate amount of hemin in the stock solution of melamine compounds. The surface of the glassy carbon electrode was then modified with 10 μL of the abovementioned liquid mixture and dried in hot air. Then, the electrode was ready to use, without any further electrochemical or chemical pre-treatment.

Results and discussion

Structural data of dendritic melamines Dim and Den

According to DFT optimization at M06-2X/def2-TZV level of theory [18], in strong hydrogen bond acceptor solvents [19] such as DMSO, **Dim** and **Den** revealed a unique and regular peripheral shape consisting of the "parallel" *anti*(↓)-*anti*(↓) (Scheme 2) [19] orientation of the two C-4, -6 *p*-hydroxyphenyl units against the third *s*-triazine *N*-ligand linked at C-2, 4,4′-bipiperidin-1-yl (in **Dim**) or piperazin-1-yl (in **Den**). This assignment originates from the well-documented character of the bonds C^{sp2}(*s*-triazine)-N(exocyclic) as partial double, due to the lpN(exocyclic) → π(*s*-triazine) conjugation [20–24]. Therefore, it was expected that the same *anti-anti* peripheral arrangement of the *p*-hydroxyphenyl units in **Dim** and **Den** remained unchanged in solid state, as in the case of other reported *N*-substituted amino-*s*-triazines [24].

Compound **Dim** had an almost planar structure due to the "chair to chair" anancomeric [25] (rigid)[1] conformation of the central linker, 4.4′bipiperdine. By contrast, piperazine, the internal linker in **Den**, was chair ⇄ chair flipping, in solution. In spite of this flexibility, the DFT optimization at M06-2X/def2-TZV level of theory of G-2 melamine dendrimer predicted a global vaulted shape in DMSO to be kept as well in solid state (Fig. 1).

[1] According to the definition from Ref.[25], rigid is "fixed in a single conformation either by geometric constraints or because of an overwhelmingly one-sided conformational equilibrium."

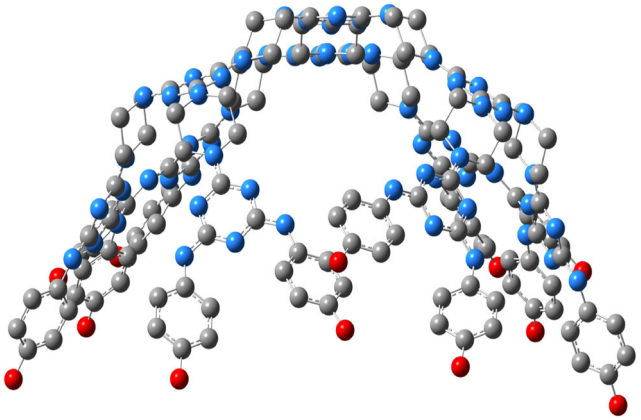

Fig. 1 The optimized geometry structure of compound **Den** obtained at M06-2X/def2-TZV level of theory (the H atoms were omitted for reasons of simplicity) [18]

FT-IR analysis

The FT-IR spectra obtained for solid mixtures containing **Hm-Dim** or **Hm-Den** in 5:1 molar ratio were compared with those of pure compounds **Dim**, **Den**, and **Hm** (Fig. 2). The vibrational analysis revealed intermolecular interactions, in solid state, between **Hm** and **Dim** or **Den**, respectively. They can be grouped as (**a**) intermolecular H-bond interactions, (**b**) proton-interchange, and (**c**) π-π stacking relationship.

As expected, the H-bond interactions involved, primarily, the OH phenolic groups of **Dim** and **Den**. In pure **Dim** and **Den**, these groups exhibited large stretch bands, around 3400 cm^{-1}, consistent with the existence of compounds, in solid state, as polymeric Ar-O(H)…H…O-Ar, i.e., $(anti\text{-}anti)_n$, networks. Addition of a 400 % molar excess of **Hm** promoted a significant shifting upfield of the ν_{OH} absorptions (about 100 cm^{-1}) due, most likely, to the in-between intercalation of the **Hm** peripheral carboxyl groups as H-bond donor-acceptor competitors (see later discussion). This shifting was more important if the melamine was *planar* (**Hm-Dim** vs. **Dim**, Fig. 2a) rather than *vaulted* (**Hm-Den** vs. **Den**, Fig. 2b). Here, we note the position of the NH stretching band, around 3300 cm^{-1}, in agreement with the intramolecular lpN(*s*-triazine)…H…N(exocyclic) association [20–24], hence irrelevant for the present discussion.

According to literature [26], the **Hm** sharp strong band located at 1700 cm^{-1} were attributed, classically, to the C=O stretch in the carboxylic acid groups. After the 400 % molar excess mixing of **Hm** with dimeric melamine G-0 dendron **Dim**, this band was shifted at 1706 cm^{-1} (still strong) and partially split into additional two weaker bands, at 1737 and 1651 cm^{-1} (Fig. 2a). A similar but complete splitting was previously noticed and assigned by Tom and Pradeep [27, 28] in the case of IR spectra of **Hm** (KBr matrix) immobilized on Au and Ag nanoparticles.[2] Following this example, the band at 1737 cm^{-1} were assigned to C=O stretch of the H-bonded free carboxylic acid group [27]; meanwhile, the band at 1651 cm^{-1} disclosed the same C=O stretch in carboxyl groups bounded to **Dim**, as carboxylate anion [26] (reported pK_a of **Hm** = 6.63 [29], 4.8–5.7 [30]). Surprisingly, the above splitting was re-found more important in the IR spectrum of mixture **Hm-Den** because $\nu_{C=O}$ (1700 cm^{-1}, strong in pure **Hm**) was shifted to 1703 cm^{-1} and divided as 1736 and 1652 cm^{-1} in **Hm-Den**. One can easily observe that all three $\nu_{C=O}$ normalized absorbance in **Hm-Den** were about four times weaker in comparison with that in pure **Hm**. That is, the proton interchange was, by far, significant in **Hm-Den** mixture with respect to that revealed by **Hm-Dim** one. The major structural differences between melamines **Dim** and **Den** consisted mainly on their size (Scheme 2) and global shape, *planar* against *vaulted*, respectively; at this stage of our knowledge, we hypothesized a partial encapsulation of planar **Hm** (an already published [31–34] aptitude of this metaloporphyrine) by a multi-branched structure [31] such as **Den**, creating a new potential metal-organic framework (MOF) [32–34].

The nature of π-π stacking relationships in metaloporphyrines is very well documented [35]. In the case of **Hm-Dim** and **Hm-Den** mixtures (Fig. 2), important normalized absorbance changes and shifting were observed in the IR region 800–1600 cm^{-1}, suggesting π-π stacking interactions between **Hm** and melamine partners. They implied, simply, the π-excessive pyrrole units (in **Hm**) as donors against π-deficient *s*-triazines (in **Dim** or **Den**) as acceptors. If so, this assignment completes those above, namely H-bond and proton interchange.

Cyclic voltammetry

First, the electrochemical behavior of glassy carbon electrodes modified with the abovementioned compounds was investigated by cyclic voltammetry. Figure 3 shows the cyclic voltammograms recorded in phosphate buffer (pH 7.0) at **GC/Dim** and **GC/Den** modified electrodes. For a comparative study, the voltammogram recorded at the unmodified glassy carbon (**GC**) electrode are also presented.

In the absence of hemin (**Hm**), no redox peaks were of notice over the entire investigated potential domain. Addition of hemin determined the appearance of a clear pair of redox peaks which can be attributed to the Fe(II)/Fe(III) redox couple existent inside the hemin molecule, i.e., a typical behavior for a porphyrinic structure.

It should be emphasized that the formal potentials of the Fe(II)/Fe(III) redox couple ($E^{o\prime}$, estimated as the average value

[2] $\nu_{C=O}$ 1700 cm^{-1} (in free **Hm**) but 1713 and 1664 cm^{-1} in **Hm** immobilized on Au, Ag(I), and Ag(II) nanoparticles [27, 28].

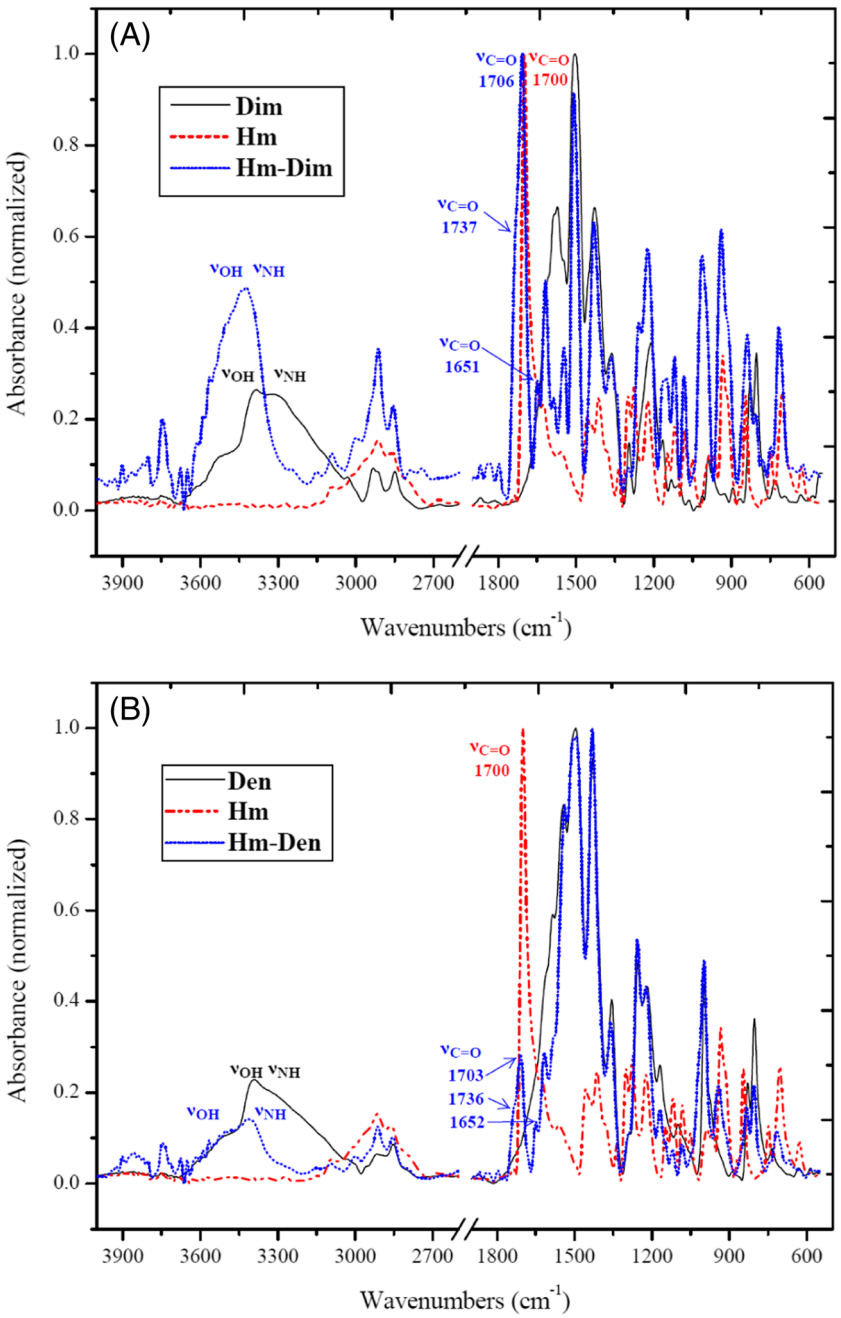

Fig. 2 Comparative FT-IR spectra (KBr) of compounds **Dim**, **Hm** against their 5:1 molar mixture **Hm-Dim** (**a**); **Den**, **Hm** against their 5:1 molar mixture **Hm-Den** (**b**)

of the anodic and cathodic peak potentials) is influenced by the immobilization matrix (Table 1). The different formal potentials of the redox couple noticed in the case of **GC/Hm-Den** and **GC/Hm-Dim** electrode ($E^{o\prime} = -0.271$ and -0.340 V, respectively) reflect the matrix-dependent behavior of **Hm**, caused by (1) the different orientations of the immobilized mixture of molecules on the electrode surface and (2) by interactions occurring between **Hm** and **Dim** or **Den** molecules, as revealed by FT-IR data. Thus, the communication between Fe(II)/Fe(III) redox centers of immobilized hemin and the electrode material took place differently.

The dependence of the anodic and cathodic peak currents on the scan rate was also investigated (Fig. 4) in a large range of scan potentials (10–1000 mV s^{-1}).

The peak potential difference ΔE_{peak} at **GC/Hm-Dim** and **GC/Hm-Den** was smaller than at **GC/Hm**, indicating that the redox reaction has an improved reversibility in the first two cases. In the absence of melamine species, used as immobilization matrix for **Hm**, the slope values of log *I* versus log *v* plot were close to 0.5, indicating a diffusion-controlled process. As expected, for **GC/Hm-Dim** and **GC/Hm-Den**, the dependence *I* versus *v* plots was linear (Fig. 4b) and the slope

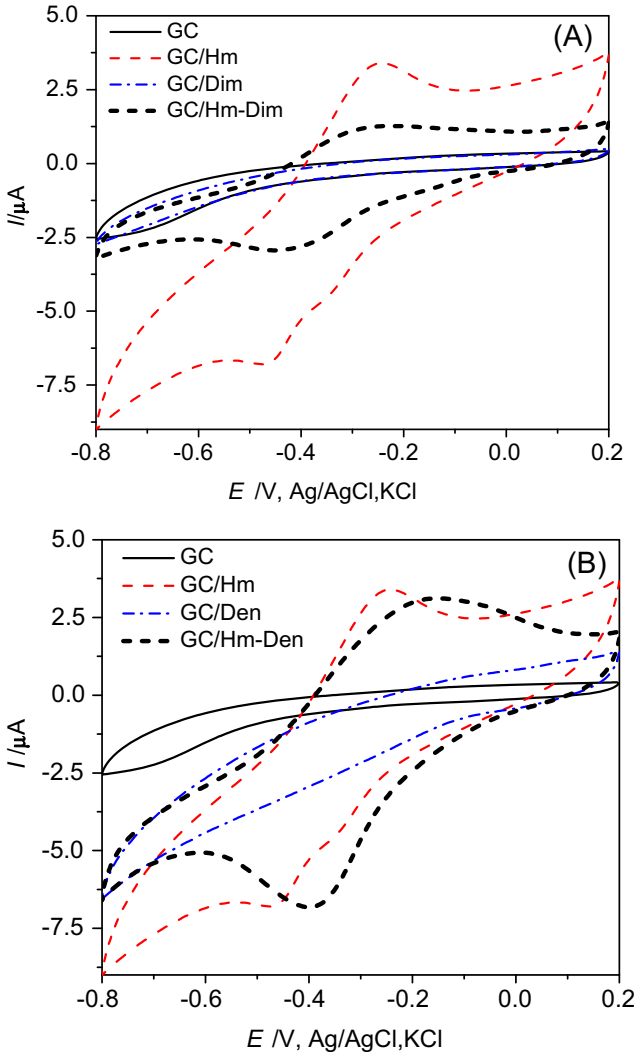

Fig. 3 **a** Cyclic voltammograms (2nd cycle) at **GC**, **GC-Hm**, **GC/Dim**, **GC/Hm-Dim** and **b** cyclic voltammograms at **GC**, **GC-Hm**, **GC/Den**, **GC/Hm-Den**, respectively. Experimental conditions: electrolyte, 0.1 M, phosphate buffer (pH 7); scan rate: 50 mV s^{-1}; starting potential, 0.2 V

values of log *I* versus log *v* plots were close to 1 (Table 1), symptomatic of the presence of a surface-confined redox couple. Deviations observed in the case of anodic peak corresponding to **GC/Hm-Den** electrodes could be due to a certain

Table 1 Parameters of the log-log linear regressions corresponding to the peak current (A) dependencies on the potential scan rate (V s^{-1}) for **GC/Hm/Dim** and **GC/Hm/Den** electrodes (experimental conditions—see Fig. 4)

Electrode	Slope		R^2/n	
	Oxidation	Reduction	Oxidation	Reduction
GC/Hm	0.515 ± 0.006	0.779 ± 0.044	0.9995/9	0.9905/8
GC/Hm-Dim	0.915 ± 0.022	0.994 ± 0.025	0.9955/9	0.9951/9
GC/Hm-Den	0.723 ± 0.052	0.936 ± 0.020	0.9996/9	0.9964/9

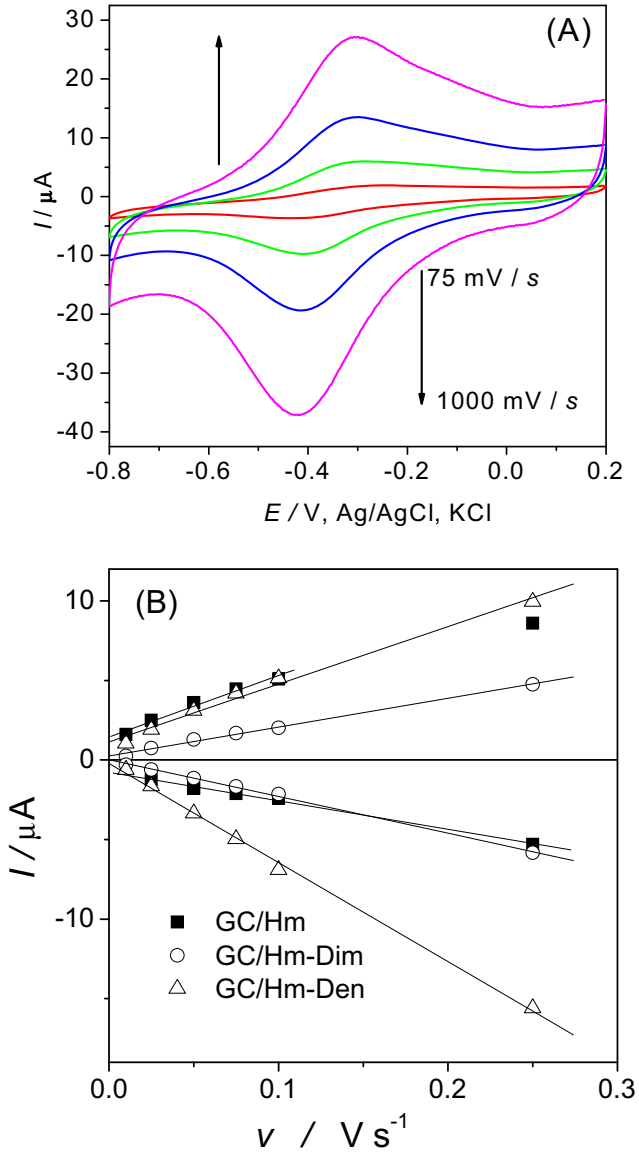

Fig. 4 The cyclic voltammograms of **GC/Hm/Dim** electrode at different scan rates (**a**) and the corresponding influence of scan rate on the current intensity (**b**) for **GC/Hm**, **GC-Hm-Dim**, and **GC/Hm-Den** electrodes. Experimental conditions: electrolyte, 0.1 M, phosphate buffer (pH 7); scan rates, see *inset*; starting potential, 0.2 V vs. Ag/AgCl, KCl_{sat}

contribution of the diffusion to the voltammetric response, especially at high scan rates.

The values of $\left| I_a/I_c \right|$ ratio were also close to 1, indicating that the electrochemical process taking place at the electrodes was quasi-reversible (Table 2). This fact was confirmed as well by the relatively small variation of ΔE_{peak} with the scan rate (results not shown).

From data listed in Table 2, one can see that the surface coverage was larger than the value corresponding to a hemin monolayer (7.5×10^{-11} mol cm^{-2}) [3] indicating the formation of more than one monolayer of hemin. However, this value was in agreement with those already reported in the literature for hemin modified surfaces [36].

Table 2 Electrochemical parameters of voltammetric response for **GC/Hm**, **GC/Hm-Dim**, and **GC/Hm-Den** modified electrodes (experimental conditions—see Fig. 3)

Electrode	ΔE_{peak} (V)	E_{FWHM} (V)		$E^{0'}$ (V/Ag/AgCl/KCl)	$\lvert I_a/I_c \rvert$	Surface coverage[a] (mol cm^{-2})	
		Anodic	Cathodic			Anodic	Cathodic
GC/Hm	0.194	0.235	0.173	−0.350	1.870	2.83×10^{-9}	9.15×10^{-10}
GC/Hm-Dim	0.140	0.169	0.128	−0.349	1.189	1.27×10^{-9}	7.66×10^{-10}
GC/Hm-Den	0.177	0.117	0.210	−0.271	0.933	3.21×10^{-9}	2.30×10^{-9}

[a] Calculated from under the peak areas recorded during the CV measurements at (50 mV s^{-1}) scan rate, using the equation $\Gamma = \frac{S_{peak}}{zFA}$ [S_{peak} = under peak area (C); A = geometric electrode surface; z = number of transferred electrons; F = Faraday's constant (C mol^{-1})]

The peak width at half peak height (E_{FHWM}) was found to be higher than that corresponding to the ideal case (E_{FHWM} = 90.6/n mV), proving the existence of repulsive interactions between the surface-confined redox species.

Rate constants for the heterogeneous electron transfer process (k_s, s^{-1}) corresponding to the Fe(III)/Fe(II) redox couple of Hm at **GC/Hm-Dim** and **GC/Hm-Den** electrodes were estimated using Laviron's treatment for the voltammetric response of adsorbed species when ΔE_{peak} <200/n mV and α = 0.5 [37].

Thus, the average electron transfer constants for **GC/Hm-Dim** and **GC/Hm-Den** electrodes were 0.556 ± 0.270 s^{-1} and 0.334 ± 0.103 s^{-1}, respectively. These values were lower than those for other hemin-modified electrodes such as hemin immobilized on MCWT [38] or on glassy carbon modified with PAMAM and MWCNT [39], probably due to the different orientation of hemin molecules on the electrode surface which influences the charge transfer rate [7]. Due to the same reason, the electrode reaction was faster when **Hm** was immobilized with **Dim** than with **Den** layer. In spite of this, the lower activity of our modified electrodes **GC/Hm-Dim** and **GC/Hm-Den** was compensated by their good stability.

Thus, the electrochemical stability of **GC/Hm-Dim** and **GC/Hm-Den** electrodes, evaluated under potentiodynamic conditions by repetitive cyclic voltammetry measurements (50 cycles), was investigated in phosphate buffer solutions of pH 7, at 50 mV s^{-1} potential scan rate. For both **GC/Hm-Dim** and **GC/Hm-Den** electrodes, the shape of the voltammograms remained invariant during cycling, proving a very good stability and a small variation of surface concentration, as illustrated in Fig. 5 for **GC/Hm-Den** electrodes. The current of the 50th cycle represented 84 % from the anodic current and 95 % from the cathodic current recorded in the first cycle, respectively.

The electrode deactivation process obeyed zero-order kinetics as confirmed by the Γ–t dependence analysis, observed in the time range 0–2500 s. The low values of the deactivation rate constants of **GC/Hm-Dim** and **GC/Hm-Den** electrodes [$(k_{deact})_{\mathbf{GC/Hm/Dim}} = 1.7 \times 10^{-13} \pm 0.360 \times 10^{-13}$ mol cm^{-2} s^{-1}, $R/n = 0.8855/8$; $(k_{deact})_{\mathbf{GC/Hm/Den}} = 1.17 \times 10^{-13} \pm 0.360 \times 10^{-13}$ mol cm^{-2} s^{-1}, $R/n = 0.7721/9$], estimated from the cathodic peak currents, proved a better chemical stability as compared with **GC/Hm** electrode [$(k_{deact})_{\mathbf{GC/Hm}} = 9.44 \times 10^{-13} \pm 0.380 \times 10^{-13}$ mol cm^{-2} s^{-1}; $R/n = 0.9788/30$]. The better stability can be assigned as due to the presence of the melamines **Dim** and **Den**, which contribute to a better immobilization on the GC surface through intermolecular interactions in solid state between **Hm** and these compounds (H-bond interactions, proton-interchange, and π-π stacking interactions). As expected, due to the stronger interactions between **Hm** and **Den**, evidenced by FT-IR analysis, the stability of the **GC/Hm-Den** was slightly higher than that of **GC/Hm-Dim** electrode.

Electrochemical impedance measurements

With the aim of assessing electrode activity, Nyquist impedance diagrams were also recorded at the different modified electrodes in the presence of $[Fe(CN)_6]^{3-}/[Fe(CN)_6]^{4-}$ redox probe in solution (Fig. 6).

In order to obtain the steady-state potential values necessary for the EIS measurements, prior to the recording of

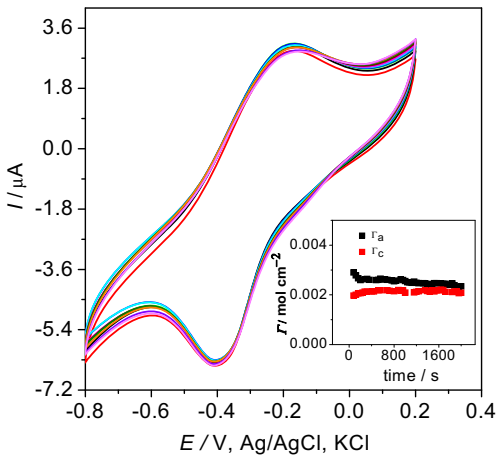

Fig. 5 The stability of **GC/Hm/Den** reflected in repetitive voltammograms (**a**) and in the variation of peak currents in time (**b**). Experimental conditions: electrolyte, 0.1 M, phosphate buffer (pH 7), scan rate, 50 mV s^{-1}; starting potential, 0.2 V vs. Ag/AgCl, KCl$_{sat}$

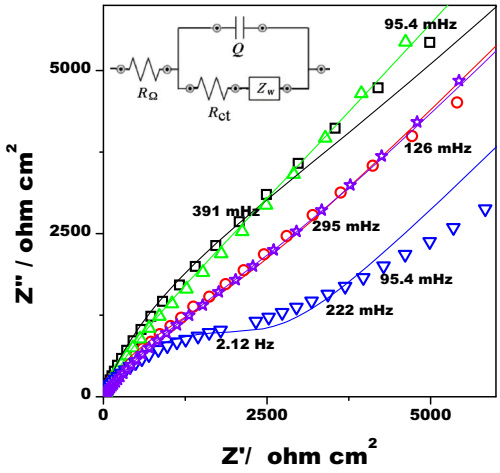

Fig. 6 Nyquist impedance diagrams for **GC** (□), **GC/Dim** (○), **GC/Hm-Dim** (Δ), GC/Den (▽), and **GC/Hm-Den** (☆) modified electrodes recorded at the open circuit potential after immersion in 0.1 M KCl + 0.05 mM $[Fe(CN)_6]^{3-}/[Fe(CN)_6]^{4-}$ solution. *Inset*: equivalent electric circuit type R(Q(RW)), used for the modeling of un/modified electrodes.

impedance spectra, open circuit potential (OCP) versus time measurements were performed.

One can observe that the system exhibited diffusion-like behavior dominant at low frequencies. Unsurprisingly, the presence of compounds **Dim** and **Den** on the electrode surface brought a significant increase of both the real and the imaginary component of the impedance to suggest that the melamine derivatives adsorbed on the electrode surface hindered the penetration of $[Fe(CN)_6]^{3-}/[Fe(CN)_6]^{4-}$ redox couple. On the other hand, due to its low conductivity, the adsorbed hemin contributed as well to the impedance increase [40].

The impedance spectra were analyzed by considering the equivalent circuit (R(Q(RW))), widely used in the literature to describe the processes taking place at modified electrode surfaces, shown in the inset of Fig. 6 [41]. The circuit contains information about the charge transfer step and the diffusion taking place at the electrode interface. It includes two resistances (R_Ω and R_{ct}) and one constant phase element (*CPE*) in combination with Warburg impedance (Z_W). R_Ω is the uncompensated solution resistance, while R_{ct} provides the value of the charge transfer resistance, corresponding to the $[Fe(CN)_6]^{3+}/[Fe(CN)_6]^{2+}$ redox couple.

The EIS spectra were modeled by fitting the experimental data with the ZSimpWin 3.21 software, and the estimated values listed in Table 3 had an error distribution less than 15 %. The Q value was modeled as a non-ideal capacitor of capacitance C with an exponent n, which equals 1 for an ideal capacitor [42]:

$$C = Q^{1/n}\left(\frac{R_\Omega R_{ct}}{R_\Omega + R_{ct}}\right)^{(1-n)/n}$$

As shown in Table 3, the **GC/Hm** electrode exhibited the R_{ct} value of 4640 Ω cm^2. The relatively high value was due mainly to the insulating character of the hemin [40]. R_{ct} decreased when single melamines **Dim** or **Den** covered the GC surface, suggesting their aptitude as better electron conductor than hemin. At the same time, the increase of the charge transfer resistance of the redox probe in the presence of hemin incorporating melamines **Dim** or **Den** against that of **GC/Den** and **GC/Dim** electrodes could be due to a blocking of an electrode part of the surface by the insulating **Hm**, formerly available for the $[Fe(CN)_6]^{3-}/[Fe(CN)_6]^{4-}$ couple. The charge transfer resistance (R_{ct}) values were higher in the presence of **Den** than in the presence of **Dim** on the **GC** surface, suggesting that the **Dim** molecules' arrangement on the electrode surface was less compact than in the other case due to their smaller dimensions and the more convenient (plane) geometry favoring the electron transfer. The n values associated to *CPE* were also different in the two cases, which can be explained as well by a change in film morphology and roughness. These last ones deviate from the perfect capacitor behavior (corresponding to $n = 1$).

The results also indicate that both melamine films act as physical barriers which hindered the penetration of $[Fe(CN)_6]^{3-}/[Fe(CN)_6]^{4-}$ redox couple towards the electrode surface (see the Z_W values related to the diffusion limited processes).

Electrocatalytic activity toward H_2O_2 reduction

In order to check the electrocatalytic activity of **GC/Hm-Dim** and **GC/Hm-Den** electrodes towards H_2O_2 reduction, their cyclic voltammetric responses were recorded in the absence and in the presence of 5×10^{-5} M H_2O_2 (Fig. 7).

It can be observed that there is a strong increase of the cathodic current at **GC/Hm-Dim** and **GC/Hm-Den** electrodes as compared with the bare **GC** and **CG/Dim** or **CG/Den** electrodes, proving the electrocatalytic effect of the modified electrodes.

The below possible mechanism for the observed electrochemical catalytic reaction was inspired by the known behavior of other Fe^{3+} containing proteins [43]:

$$\text{Hemin}\left(Fe^{3+}\right) + H^+ + e^- \rightarrow \text{Hemin}\left(Fe^{2+}\right)$$

$$\text{Hemin}\left(Fe^{2+}\right) + H_2O_2 + 2H^+ + e^- \rightarrow \text{Hemin}\left(Fe^{3+}\right)$$

The catalytic efficiency of the modified electrodes [calculated as CE (%) = $(I_{pc,H2O2} - I_{pc,0})/I_{pc,0}$, where $I_{pc,0}$ is the cathodic peak current recorded in the absence of H_2O_2 and $I_{pc,H2O2}$ is the cathodic peak current recorded in the presence of H_2O_2, respectively] was 77.66 % for **GC/Hm-Dim** and 64.98 % for **GC/Hm-Den**. The magnitude of these values revealed that hemin had good catalytic and intrinsic

Table 3 Electrochemical impedance spectroscopy data of GC, GC/Dim, **GC/Hm-Dim**, GC/Den, and **GC/Hm-Den** modified electrodes after immersion in $[Fe(CN)_6]^{3+}/[Fe(CN)_6]^{2+}$, using a *R(Q(RW))* equivalent electric circuit (experimental conditions—see Fig. 6)

Electrode	*OCP* V vs. RE	R_Ω (Ω cm^2)	Q (Ω^{-1} s^n cm^{-2})	n	R_{ct} (Ω cm^2)	W (Ω^{-1} s$^{0.5}$ cm^{-2})	C (μF cm^{-2})	χ^2
GC/Hm	0.091	8.82 ± 2.65	7.01 10^{-5} ± 4.34	0.819	4640 ± 11.34	15.34 10^{-5} ± 3.55	13.68	0.00360
GC/Dim	0.128	7.67 ± 3.11	4.73 10^{-5} ± 5.17	0.806	1845 ± 7.480	22.71 10^{-5} ± 2.17	7.02	0.00272
GC/Hm-Dim	0.023	14.88 ± 2.02	11.53 10^{-5} ± 4.98	0.766	3409 ± 17.35	15.40 10^{-5} ± 3.27	16.46	0.00237
GC/Den	0.153	5.51 ± 15.93	2.77 10^{-5} ± 7.43	0.727	2541 ± 4.95	48.61 10^{-5} ± 4.43	1.02	0.00690
GC/Hm-Den	0.081	11.02 ± 6.53	7.17 10^{-5} ± 4.77	0.616	4747 ± 10.59	12.35 10^{-5} ± 3.15	0.83	0.00166

The RSD for each parameter is expressed in %; *W* is the reciprocal Warburg coefficient

peroxidase-like activity that can facilitate the reduction of H_2O_2.

In what the reproducibility of these results is concerned, the cyclic voltammograms, recorded in 0.1 M phosphate buffer (pH 7) containing 0.8 μM H_2O_2 at three different **GC/Hm-Den** electrodes, provided, for the H_2O_2 cathodic peak potential, an average value of −0.423 ± 0.006 V versus Ag/AgCl, KCl_{sat} (RSD = 1.32 %) and, for the cathodic peak current, an average value of 1.048 ± 0.156 μA (RSD = 14.9 %). These values recommend the **GC/Hm-Den** modified electrode as a valuable sensor for the voltammetric detection of H_2O_2.

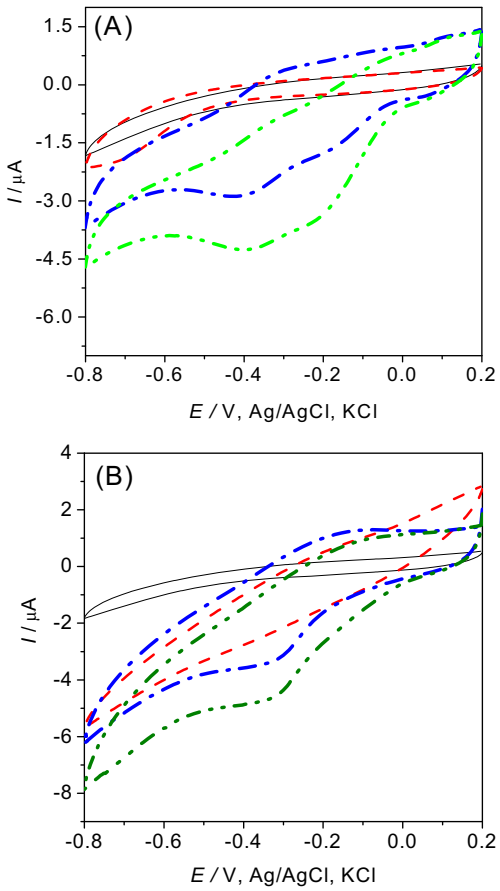

Fig. 7 Cyclic voltammograms of 0.05 mM H_2O_2 at **GC** (**a**, **b**, solid line), **GC/Dim** (**a**, *dash line*), **GC/Den** (**b**, *dash line*), **GC/Hm-Dim** (**a**, *dash-dot-dot line*), and **GC**/Hm-**Den** (**b**, *dash-dot-dot line*) electrodes. The *dash-dot lines* correspond to **GC/Hm-Dim** (**a**) and **GC/Hm-Den** (**b**) electrodes in the absence of H_2O_2. Experimental conditions: electrolyte, 0.1 M, phosphate buffer (pH 7); scan rate, 50 mV s^{-1}; starting potential, 0.2 V vs. Ag/AgCl, KCl_{sat}

Amperometry

Amperometric measurements allowed the determination of the electroanalytical parameters of the modified electrodes. Figure 8 shows the typical calibration curves obtained by amperometry at an applied potential of −0.35 V versus Ag/AgCl, KCl_{sat} for successive injections of H_2O_2. The substrate concentrations were changed by stepwise addition of a concentrated solution to a stirred buffer, allowing steady-state current responses which are very stable and fast, having a 20 s response time ($t_{95\%}$). In Fig. 8, I_c is the cathodic current measured at each concentration after stabilization of the current and I_0 is the cathodic current in the absence of H_2O_2.

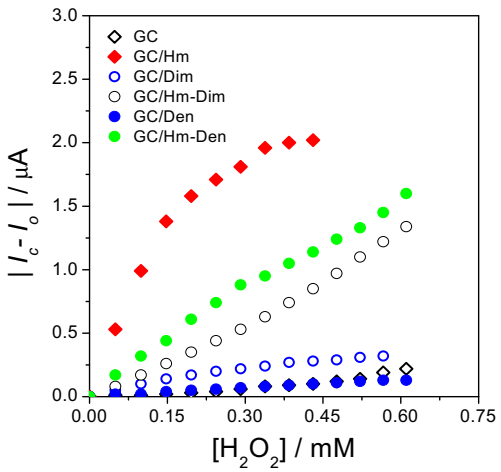

Fig. 8 Calibration curves for H_2O_2 detection at GC (**a**, **b**, □), **GC/Hm** (**a**, **b**, ■), **GC/Dim** (**a**, ○), **GC/Den** (**b**, ○), **GC/Hm-Dim** (**a**, Δ), and **GC/Hm-Den** (**b**, Δ) modified electrodes. Experimental conditions: electrolyte, 0.1 M, phosphate buffer (pH 7); applied potential, −0.35 V vs. Ag/AgCl, KCl_{sat}; stock H_2O_2 concentration, 10^{-2} M; continuous stirring

Table 4 The analytical parameters for H_2O_2 detection at **GC/Hm-Den** and **GC/Hm-Dim** (experimental conditions—see Fig. 6)

Electrode	Sensitivity (mA/M)	Detection limit[a] (μM)	Linear range (μM)	*R*/*n*
GC	0.257 ± 0.016	53.9	0–476	0.9654/11
GC/Hm	8.190 ± 0.715	31.6	0–170	0.9888/5
GC/Dim	0.820 ± 0.046	25.0	0–250	0.9937/6
GC/Den	0.224 ± 0.035	20.9	0–566	0.9977/13
GC/Hm-Dim	1.909 ± 0.032	11.9	0–400	0.9979/9
GC/Hm-Den	2.762 ± 0.090	22.0	0–400	0.9964/9

[a] Calculated as $3s_a/b$, where s_a is the standard deviation of the intercept of the calibration curve $I = a + b[H_2O_2]$ and b is the slope of the calibration curves [46]

The analytical parameters of the **GC/Hm-Den** and **GC/Hm-Dim** modified electrodes are presented in Table 4.

The evaluation of the analytical parameters of the studied electrodes reveals that the presence of **Hm** in the composite matrix on the electrode surface enhanced the sensitivity and decreased the detection limit for H_2O_2, if compared with the unmodified **GC**, **GC/Den**, or **GC/Dim**. Moreover, the melamine compounds alone also had a beneficial effect on the **GC** electrode activity. Best electroanalytical parameters were obtained in the case of **GC/Hm-Dim** electrode, probably due to the more convenient steric orientation of the hemin units against the electrode surface, which allow a better communication between its redox centers and the glassy carbon substrate. A certain contribution to the catalytic behavior could have the dimer itself, which was proven to be electroactive in DMSO due to the peripheral phenolic groups present in its structure [17].

The analytical parameters for H_2O_2 detection at **GC/Dim-Hm** and **GC/Den-Hm** are in accordance with other values previously reported in literature [7].

In what the selectivity of the electrode is concerned, the study of common interferents such as uric acid and ascorbic acid by analyzing the amperometric response to successive spikes of 500 μL from a 10^{-2} M solution of these interferents in 10 mL buffer solution, at an applied potential of −0.35 V, showed no significant alteration of the current signal (see Fig. SM-9 in the supplementary material).

Conclusions

We reported the use of two new *N*-substituted melamines as matrices for the immobilization of hemin on glassy carbon substrate: a new G-2 melamine dendrimer (2,4,6-triamino-1,3,5-triazine) comprising *p*-aminophenol as peripheral unit (**Den**) and one of its analogues, a melamine G-0 dimer (**Dim**). In solid state, FT-IR analysis revealed intermolecular interactions between **Hm** mixed with **Dim** or **Den** which could support the different behavior of GC-modified electrodes based on different combinations of these compounds.

Measurements carried out by cyclic voltammetry and electrochemical impedance spectroscopy allowed the estimation of electrochemical parameters of **GC/Hm**, **GC/Hm-Dim**, and **GC/Hm-Den** electrodes. For the redox process taking place at these electrodes, the heterogeneous electron-transfer rate constants (k_s, s^{-1}) were estimated using the Laviron treatment.

Both modified electrodes exhibited good stability and catalytic activity toward H_2O_2 reduction. Amperometric measurements allowed determining the electroanalytical parameters of the modified electrodes. The **GC/Hm-Dim** electrode exhibited higher catalytic properties than **GC/Hm-Den** electrode, but lower stability.

Acknowledgments The financial support from a grant provided by the Research Council Romania (Project PN-II-ID-PCE-2011-3-0128) is gratefully acknowledged. A.B. acknowledges the financial support from the Romanian National Authority for Scientific Research and Innovation (ANCSI) through the Core Program 2015.

References

1. Chen J, Zhao L, Bai H, Shi G (2011) J Electroanal Chem 657:34–38
2. Sosna MJ, Fapyane D, Ferapontova EE (2014) J Electroanal Chem 728:18–25
3. Brusova Z, Magner E (2009) Bioelechem 76(1–2):63–69
4. Bruice TC (1991) Acc Chem Res 24:243–249
5. Ni Y, Wang P, Song H, Lin X, Kokot S (2014) Anal Chim Acta 821: 34–40
6. Santos RM, Rodrigues MS, Laranjinha J, Barbosa RM (2013) Biosens Bioelectron 44:152–159
7. Valentini F, Cristofanelli L, Carbone M, Palleschi G (2012) Electrochim Acta 63:37–46
8. Song H, Ni Y, Kokot S (2013) Anal Chim Acta 788:24–31
9. Wong A, Materon EM, Del Pilar Taboada Sotomayor M (2014) Electrochim Acta 146:830–837
10. Zeng F, Zimmerman SC (1997) Chem Rev 97:1681–1712
11. Balzani V, Ceroni P, Giansante C, Vicinelli V, Klarner FG, Verhaelen C, Vogtle F, Hahn U (2005) Angew Chem Int Ed 44: 4574–4578
12. Newkome GR, Woosley BD, He E, Moorefield CN, Guther R, Baker GR, Escamilla GH, Merrill J, Luftmann H (1996) Chem Commun 24:2737–2738
13. Jockusch S, Turro NJ, Tomalia DA (1995) Macromolecules 28: 7416–7418
14. Alonso B, Moran M, Casado CM, Lobete F, Losada J, Cuadrado I (1995) Chem Mater 7:1440–1442
15. Bustos Bustos E, Chapman TW, Rodriguez-Valadez F, Godinez LA (2006) Electroanal 18:2092–2098
16. Lates V, Gligor D, Darabantu M, Muresan LM (2007) J Appl Electrochem 37:631–636
17. Morar C, Turdean G, Bende A, Lameiras P, Antheaume C, Muresan LM, Darabantu M (2016) Manuscript under review
18. Weigend F, Ahlrichs R (2005) Phys Chem 7:3297–3305
19. Ghiviriga I, Oniciu DC (2002) Chem Commun 22:2718–2719
20. Drakenberg T, Forsen S (1971) Chem Commun 21:1404–1405
21. Mirvish SS, Gannett P, Babcook DM, Williamson D, Chen SC, Weisenburger DD (1991) J Agric Food Chem 39:1205–1210
22. Willner I, Rosengaus J, Eichen YJ (1993) Phys Org Chem 6:29–43

23. Katritzky AR, Ghiviriga I, Oniciu DC, Barkock A (1995) J Chem Soc Perkin Trans 2(4):785–792
24. Katritzky AR, Ghiviriga I, Steel PG, Oniciu DC (1996) J Chem Soc Perkin Trans 2(3):443–447
25. Eliel EL, Wilen SH (1994) Stereochemistry of the organic compounds. John Wiley & Sons, New York, pp 642–1191
26. Parker FS (1971) Biology and medicine: applications of infrared spectroscopy in biochemistry. Plenum Press, New York, p 351
27. Tom RT, Pradeep T (2005) Langmuir 21:11896–11902
28. Wood BR, Langford SJ, Cooke BM, Lim J, Glenister KK, Duriska M, Unthank JK, McNaughton D (2004) J Am Chem Soc 126: 9233–9239
29. Hasinoff BB, Dunford HB, Horne DG (1969) Can J Chem 47: 3225–3232
30. Wu DG, Cahen D, Graf P, Naaman R, Nitzan A, Shvarts D (2001) Chem Eur J 7:1743–1749
31. Schappacher M, Deffieux A (2004) Polymer 45:4633–4639
32. Wang Q, Yang Z, Zhang X, Xiao X, Chang CK, Xu B (2007) Angew Chem Int Ed 46:4285–4289
33. Luo F, Lin Y, Zheng L, Lin X, Chi Y (2015) Appl Mater Interfaces 7:11322–11329
34. Xie S, Ye J, Yuan Y, Chai Y, Yuan R (2015) Nanoscale 7:18232–18238
35. Hunter AA, Sanders JKM (1990) Chem Rew 112:5525–5534
36. Toader AM, Volanschi E, Lazarescu MF, Lazarescu V (2010) Electrochim Acta 56:863–866
37. Laviron E (1979) J Electroanal Chem 101:19–28
38. Ye JS, Wen Y, Zhang W, Cui HF, Gan LM, Xu GQ, Sheu FS (2004) J Electroanal Chem 562:241–246
39. Ma Q, Ai S, Yin H, Chen Q, Tang T (2010) Electrochim Acta 55: 687–6694
40. Huang W, Hao Q, Lei W, Wu L, Xia X (2014) Mater Res Express. doi:10.1088/2053-1591/1/4/045601
41. Zuo G, Liu X, Yang J, Li X, Lu X (2007) J Electroanal Chem 605: 81–88
42. Hirschorn B, Orazem ME, Tribollet B, Vivier V, Frateur I, Musiani M (2010) Electrochim Acta 55:6218–6227
43. Chen G, Sun H, Hou S (2016) Anal Biochem 502:43–49